



**HAL**  
open science

## Insights on asymmetric BTB-based molecular junctions: Effect of electrode coupling

Sylvain Pitié, Mahamadou Seydou, Yannick J Dappe, Pascal Martin, François  
Maurel, Jean Christophe Lacroix

### ► To cite this version:

Sylvain Pitié, Mahamadou Seydou, Yannick J Dappe, Pascal Martin, François Maurel, et al.. Insights on asymmetric BTB-based molecular junctions: Effect of electrode coupling. *Chemical Physics Letters*, 2021, 787, pp.139273. 10.1016/j.cplett.2021.139273 . hal-03856808

**HAL Id: hal-03856808**

**<https://hal.science/hal-03856808v1>**

Submitted on 16 Nov 2022

**HAL** is a multi-disciplinary open access archive for the deposit and dissemination of scientific research documents, whether they are published or not. The documents may come from teaching and research institutions in France or abroad, or from public or private research centers.

L'archive ouverte pluridisciplinaire **HAL**, est destinée au dépôt et à la diffusion de documents scientifiques de niveau recherche, publiés ou non, émanant des établissements d'enseignement et de recherche français ou étrangers, des laboratoires publics ou privés.



# Insights on asymmetric BTB-based molecular junctions: Effect of electrode coupling

Sylvain Pitié<sup>a</sup>, Mahamadou Seydou<sup>a,\*</sup>, Yannick J. Dappe<sup>b</sup>, Pascal Martin<sup>a</sup>, François Maurel<sup>a</sup>, Jean Christophe Lacroix<sup>a</sup>

<sup>a</sup> Université de Paris, ITODYS, CNRS, Paris F-75006, France

<sup>b</sup> SPEC, CEA, CNRS, Université Paris-Saclay, CEA Saclay, Gif-sur-Yvette Cedex 91191, France

## ARTICLE INFO

### Keywords:

Electron transport  
NEGF  
DFT  
BTB  
Titanium  
Gold  
Graphene  
Attenuation factor  
Decay constant

## ABSTRACT

NEGF and DFT calculations within Fisher Lee formalism are used to explore the effect of the asymmetry and the strength of coupling with the electrode on transport properties of 1-(2-bisthiényl)benzene oligomers. Electronic analysis of metal–molecule interactions reveals the ionic nature of Ti–C bonds inducing an interfacial dipole. The Ti *d*-orbitals are found to be strongly coupled to the lowest unoccupied orbital of BTB, thus facilitating charge transfer from Ti to the molecule. The hole transport mechanism is found in the cases of Au-(BTB)<sub>n</sub>-Au and Au-(BTB)<sub>n</sub>-Ti while possible combined hole and electron transport is predicted in the case of Ti-(BTB)<sub>n</sub>-Ti.

## 1. Introduction

The possibility offered by organic molecules to mimic electronic functions (resistance, diode, transistor, switch) is at the origin of the emergence of an active disciplinary field at the interface of Chemistry and Physics [1]. They promise lower cost and probably lower electrical consumption, offering an alternative to silicon technology [2]. In this context many experimental setups have been developed with the aim of sandwiching selected molecules between electrodes and measuring their transport properties at the nanoscale [3]. Hence, while experimental setups seem to be well established, many points are still not understood and many obstacles have to be overcome before industrial production can be considered<sup>4</sup>. Among these, one can cite, the control of top molecular-electrode junction, the reliability of measurements, a detailed understanding of transport mechanisms as a function of the junction length and molecular structure. To tackle these challenges, several theoretical and numerical approaches have been developed recently to accurately determine electron transport within metal–molecule–metal junctions using quantum calculations.[4] The common approach, based on non-equilibrium Green's functions (NEGF), has given results in very good agreement with experiment. In particular, NEGF combined with density functional theory (DFT) in a fully self-consistent process makes it

possible to effectively treat the diffusion region coupled to the electrodes [5]. The coupling of experimental measurements with theoretical calculations has made it possible to interpret the transport mechanism of large ranges of conjugated molecular systems.[6–8]

Among the systems of interest, attention have been given to thiophene-based oligomers due to their favorable chemical stability, their synthetic versatility and their efficient charge transport along the highly conjugated  $\pi$ -orbitals of the oligomers.[9] As such, several studies have been conducted on pure oligothiophenes and their side or terminal group functionalization.[10–12] Indeed, Tada's group performed several studies on the synthesis and transport properties of these oligomers and showed that the conductance varies exponentially with the oligomer length.[10,11] Conversely, other authors found a significant deviation in conductance with length due to conformational change for some oligomers.[12,13] Xiang *et al.*[14] used iodine to functionalize thiophene-based oligomers and found a non-exponential variation of the conductance with the molecular length, that they attributed to modification of the frontier orbital levels. Combining theoretical calculations and experiments, Leary *et al.* explored solvent effects on oligothiophenes and showed that the molecular conductance is over 2 orders of magnitude larger in the presence of a shell comprising 10 water molecules. [13] More recently, Li *et al.*[15] investigated charge transport through

\* Corresponding author.

E-mail address: [mahamadou.seydou@u-paris.fr](mailto:mahamadou.seydou@u-paris.fr) (M. Seydou).

<https://doi.org/10.1016/j.cplett.2021.139273>

Received 27 July 2021; Received in revised form 1 December 2021; Accepted 2 December 2021

Available online 7 December 2021

0009-2614/© 2021 Elsevier B.V. All rights reserved.

intermolecular and intramolecular paths in single-molecule and single-stacking thiophene junctions using the mechanically controlled break-junction (MCBJ) technique. They concluded that intermolecular charge transport offers the efficient and dominant path at the single-molecule scale. Even if experimental and theoretical developments progress, full understanding of the transport mechanism remains a challenge due to the time limits of calculations, the complexity of the oligomer conformations and their coupling to the electrodes.

In this work, we have introduced the Fisher-Lee approach [16] in a DFT code as implemented in Fireball [17] allowing the possibility to explore the electronic transport properties of large size systems with good accuracy in a short computing time, owing to the Fireball characteristics. First, we use this approach to determine the attenuation factors of a range of benchmark molecular systems taken from literature. In the non-resonant tunneling regime the conductance  $G$  varies exponentially with the molecular length  $L$  ( $G = G_c e^{-\beta L}$ ), where  $\beta$  is the attenuation factor, also called the decay constant, and  $G_c$  is the contact conductance, equal to the inverse of the contact resistance  $R_c$ . The attenuation factor characterizes the conduction capacity of a molecular chain. This quantity depends both on the nature of the molecular system and on its connection to the electrodes. Its value varies for conjugated molecules between 2 and 3 nm<sup>-1</sup> and it has been proved that the coupling strength to the electrodes allows to modulate its value [18]. The contact resistance  $R_c$  is known to be primarily dependent on the surface structure and the specific interaction site between the molecule and the surface [19]. Experiments on molecular junctions are carried out under different conditions, and similarly, from a theoretical point of view, calculations are made on electrodes ranging from small clusters to the ideal periodic surface. Under these very different conditions, direct comparison between contact resistances is very delicate. Thus, we prefer to focus on the attenuation factor. The results obtained are compared to experiments and other theoretical studies as a benchmark of our implementation. Secondly, we explore the electron transport properties in linear polymeric oligo(1-(2-bisthiényl)benzene) (BTB) sandwiched between titanium, gold and graphene electrodes. The attenuation factor and the charge transport mechanism were determined and compared to experiments carried out on this system in large-area junction as well as at the single-molecule level.[20] Finally, we used standard DFT calculations to interpret quantum transport results by evaluating the adsorption mechanism of anchoring groups on common stable surfaces (Au, Ti, graphene). This leads to a better understanding of the influence of molecule/electrode coupling on the conductance attenuation factor.

## 2. Computation methods

### 2.1. Quantum transport calculations

Quantum transport calculation have been performed within NEGF combined to tight binding Density Functional Theory (DFT) formalism as implemented in the Fireball code [17]. This code is a very efficient tool using an optimized localized orbital basis set [21], and the local density approximation (LDA) for the exchange and correlation energy through the McWeda formalism [22]. It offers a good compromise between computational time and accuracy, allowing to study large organic or hybrid organometallic systems.[23,24] A Keldysh-Green's functions approach was previously implemented in the Fireball code [25] and used mainly for STM image calculations, but also to model molecular junctions [26]. In this approach, the system is decomposed into two parts, namely the tip and the substrate [25]. This approach is limited by the choice of the frontier between the two parts, usually the bottleneck for the current flowing in the system. A possible solution consists in using the Fisher-Lee approach [16] where the molecular part and the two electrodes are clearly separated.

The implementation of Fisher-Lee formalism consists in decomposing the system into three parts (see scheme 1), namely the left and right electrodes and the central part, *i.e.* the molecule.

The Green's functions of Right and Left parts are defined by:

$$G(E)_{R,L}[(E - i\eta)1 - H_{R,L}]^{-1} \quad (1)$$

and the Green's function of the central part can be written as:

$$G_C(E)[(E - i\eta)I - H_C - \Sigma_L(E)\Sigma_R(E)]^{-1} \quad (2)$$

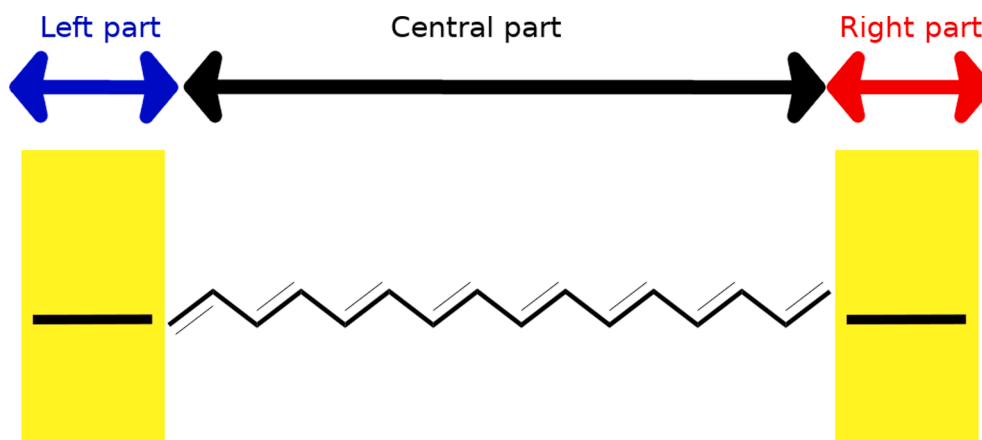
where  $\Sigma_{L,R}(E)$  are the self-energies of the electrodes and  $\eta$  is the imaginary part of the Green's function which is representative of the electronic level width or, in other words, the coupling between these levels. This parameter is used to modify the level widths of a specific subsystem, and in particular allows to distinguish the electron reservoir and the molecular channel. Hence, on one hand, the electron reservoir levels are enlarged, to take into account the bulk character, and on the other hand, the discrete molecular electronic level. We choose a value of  $\eta$  of 0.5 eV for the electrode part and 10<sup>-8</sup> eV for the molecular part.

Consequently, the transmittance  $T(E)$  is related to the advanced Green's functions through:

$$T(E) = T_r[\Gamma_L(E)G_c(E)\Gamma_R(E)G_c^\dagger(E)] \quad (3)$$

where the  $\Gamma_{R,L}$  matrices correspond to the coupling matrices between the electrodes and the central part. The transmittance spectrum can therefore be plotted for each optimized system at zero bias.

In practice, we first optimized the geometries of a family of seven



**Scheme 1.** Decomposition of the junction into three parts: left and right electrodes linked by the conjugated oligomer.

molecular junctions gathered from the literature. Once the equilibrium position was found, we determined the corresponding electronic structure by density of states (DOS) calculations. From these DOS and the hopping integrals of the system, we performed electron transport calculations.

## 2.2. Periodic DFT/PBE calculations

To analyze the nature of anchoring group bonding, we performed DFT calculations under the generalized gradient approximation (GGA) with the Perdew-Burke-Ernzerhof (PBE) functional [27] as implemented in the Vienna Ab-initio Simulation Package (VASP 5.4.4) [28] in order to model the binding of benzene and thiophene groups on Au(111), Ti (001) and graphene-based electrodes. To this end, electron-ion interactions were described by the projector augmented wave (PAW) [29] method, representing the valence electrons, as provided in the code libraries. The convergence of the plane-wave expansion was obtained using a cut-off energy of 500 eV. To adequately describe the effects of van der Waals interactions, all the computations reported in this work were performed using the dispersion-included DFT-D3 method. [30] For geometry optimization, sampling in the Brillouin zone was achieved on a  $(3 \times 3 \times 1)$  grid of k-points.

In the present study, slabs representing Au (111) and Ti (001) surfaces were cut out of the optimized bulk face-centered cubic cell of gold and a hexagonal titanium structure, respectively, using Modelview software. [31] For Au, the face-centered cubic (fcc) bulk optimized cell parameter at the PBE level was 4.08 Å, in good agreement with experiment (4.08 Å). [32] For Ti, the hexagonal bulk optimized parameter was  $a = b = 2.95$  Å and  $c = 4.68$  Å in agreement with crystallographic results. [33]

Both surfaces are modeled as a slab, where a unit cell is periodically reproduced in two dimensions ( $x, y$ ), with a vacuum space in the  $z$ -axis direction. This vacuum space size is set to 40 Å, enough to enable molecule binding and disable its interaction with the consecutive repetition of the system. In the case of Au and Ti, the slab model consists in four layers, where the two bottom layers are frozen in the optimized bulk positions and the two upper layers are relaxed. A super-cell representing a  $(3 \times 3)$  super-cell is built from the optimized Au(111) and Ti (001) and  $(5 \times 5)$  unit cells for graphene. This super-cell size allows to explore more finely the adsorption of ternary (hollow), binary (bridge) and top sites (scheme 2). One molecule is placed inside the super-cell corresponding to a coverage of  $1.1 \cdot 10^{10}$ ,  $1.5 \cdot 10^{10}$  and  $0.7 \cdot 10^{10}$  molecules/cm<sup>2</sup> for Au, Ti and G, respectively.

The binding energy is computed as the difference between the energies of optimized metal-molecule and the isolated bare metal and molecules optimized separately.

$$\Delta E_{bind} = E(Mm) - E(M) - E(m)$$

where  $E(Mm)$  is the optimized energy of the metal-molecule interface,  $E(m)$  is the optimized energy of the isolated molecule and  $E(M)$  is the energy of the bare surface.

In order to analyze bond formation, we have determined with high accuracy the charges densities of complexes, separate molecules, and bare surfaces ( $\Delta\rho(r) = \Delta\rho_{Mm}(r) - \Delta\rho_M(r) - \Delta\rho(r)_m$ ) from optimized structures by sampling the Brillouin zone on a grid of  $(9 \times 9 \times 1)$  k-points. In addition, we have calculated the Bader charges [34] on this fine grid of charge densities. Finally, we computed the work function and its variation, to highlight the formation of an interface dipole.

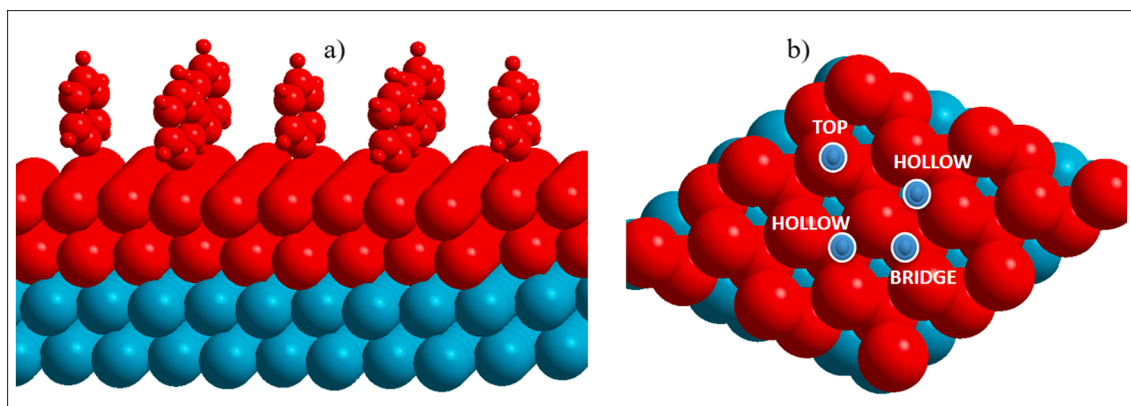
## 3. Results and discussion

### 3.1. Calculation of attenuation factor: Comparison with experiments

The implemented approach is applied to compute the decay constant and contact resistance of molecular junctions constructed from a set of seven monomers shown in Fig. 1a sandwiched between gold electrodes. These junctions are chosen according to the availability of experimental measurements of the attenuation factor. The structures as well the anchoring groups are different. Using DFT formalism as implemented in the Fireball code [17], we built the structures of the oligomers and fully optimized their geometries. From these optimized geometries, the transmittance spectra are computed using (NEGF + DFT) within the Fisher-Lee approach. In the non-resonant tunneling regime, since the transmittance  $T(E)$  varies exponentially with the length ( $L$ ) of the oligomer chain, the logarithm of the transmittance  $\text{Log}(T(E))$  varies linearly with  $L$  ( $\text{Log}(T(E)) = -\beta L + \text{Log}(R_0/R_c)$ ) where  $R_0$  is the inverse of the quantum conductance equivalent to  $h/2e^2$ . In Fig. 1b,  $\text{Log}(T(E))$  plotted as a function of  $L$  shows a linear decrease, as expected for all systems. The calculated decay constant and contact resistance are deduced from the linear fit of this line. The calculated values of  $R_c$  are compared with the experimental and theoretical ones found in the literature in Table S1. As explained earlier in the Introduction, the contact resistance  $R_c$  is not discussed here.

The investigated systems can be divided into two groups: On one hand, ONI, OPI and OPTI and BDT were experimentally investigated using conductive-probe atomic force microscopy (CP-AFM) technic. A thiol group forming the well-known Au-S bond grafted them onto the electrode. Theoretical calculations have been carried out on OPI and BTD [3536] within the framework of Landauer-Buttiker formalism. On the other hand, diaryloligoynes functionalized by BT, CN and PY as anchoring groups were studied experimentally using scanning tunneling microscopy break-junction (STMBJ) method.

Table 1 summarizes the values of the attenuation factor  $\beta$  (in nm<sup>-1</sup>)



**Scheme 2.** (a) molecule adsorbed on Au (111) super-cell showing relaxed atoms (red) and fixed atom (blue) during geometry optimization. (b) Top view of the  $(3 \times 3)$  super-cell indicating possible adsorption sites.

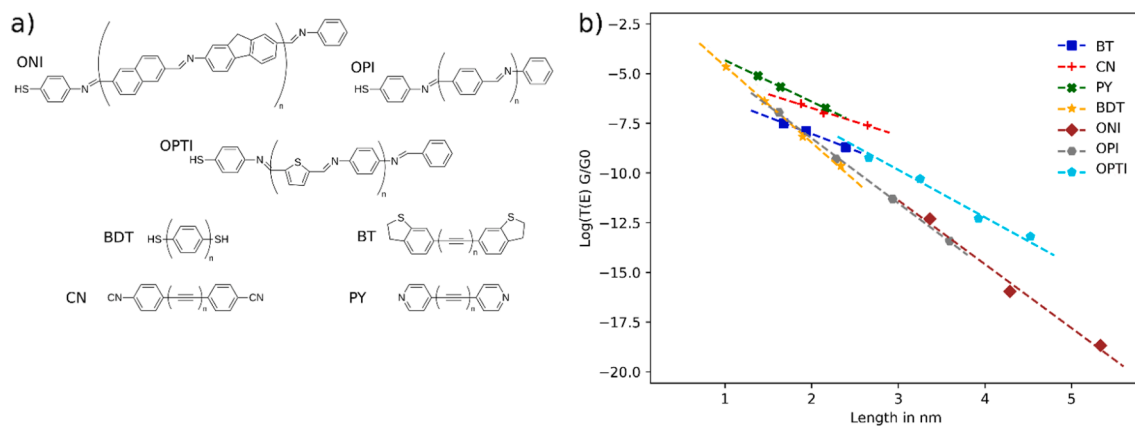


**Fig. 1.** a) Representation of the molecular systems considered for the benchmark: ONI = oligonaphthalene-fluorene-imine, OPI = oligophenylene-imine, OPTI = oligophenylene-thiophene-imine, BDT = oligophenylene, BT = dihydrobenzothiophene-oligo, CN = cyanoligo, PY = pyridyloligo. b) Plot of the corresponding transmittance at the Fermi level, as a function of the molecular length.

**Table 1**

Summary: decay constant  $\beta$  compared to experimental data and other theoretical calculations.

Systems	$\beta_{\text{exp}}$ ( $\text{nm}^{-1}$ )	$\beta_{\text{theo}}$ ( $\text{nm}^{-1}$ )	$\Delta\beta_{\text{theo-exp}}$ ( $\text{nm}^{-1}$ )	$\beta_{\text{this work}}$ ( $\text{nm}^{-1}$ )	$\Delta\beta_{\text{this work-exp}}$ ( $\text{nm}^{-1}$ )
ONI	2.5[38]	/	/	3.2	0.7
OPI	3.0[38]	2.5[39]	0.5	3.4	0.4
OPTI	3.4[35]	/	/	2.6	0.8
BDT	4.2 [36]	1.3[40]	2.9	3.9	0.3
BT	2.9[37]	1.7[37]	1.2	1.7	1.2
CN	1.7[37]	0.4[37]	1.3	1.4	0.3
PY	3.1[37]	2.2[37]	0.9	2.1	1.0

compared to experimental and other theoretical studies found in the literature. Our calculated values are in good agreement with experiment for all the systems considered, with a deviation smaller than  $1.0 \text{ nm}^{-1}$ . Overall, theoretical calculations underestimate the  $\beta$  value compared to experimental measurements. This has been observed previously and attributed to the well-known trend of DFT to underestimate the band gap, leading to an underestimation of  $\beta$ . [37] In addition, the discrepancies between our values and experimental ones seem to be related to the structure of the anchored group. In the first series, the maximum

deviation ( $0.8 \text{ nm}^{-1}$ ) is found for OPTI [35] for which the anchor group with the top electrode is a phenyl ring. In the second series, the highest deviations are obtained for the BT and PY cyclic anchoring groups with  $1.2$  and  $1.0 \text{ nm}^{-1}$ , respectively. These cyclic groups make the description of the molecule-electrode coupling less consistent. The differences with the other theoretical results originate also from the nature of the electrodes that are modeled by clusters in this work or periodic ideal surfaces in other cases. [37]

### 3.2. Attenuation FACTOR calculation for asymmetric junctions: Strength of coupling effect

The attenuation coefficient is computed through the determination of the transmittance at Fermi level depending on the length of BTB-based oligomers sandwiched between gold (Au) and different electrodes. In particular, the phenyl group of BTB is anchored to gold and the thiophene terminal group is attached to gold, titanium (Ti), and graphene (G) electrodes.

Fig. 2 shows the variations of transmittance on a logarithmic scale ( $\log(T(E))$ ) for different cases of  $(BTB)_2$  junctions when the right electrode is modified. The transmittances at the Fermi level are  $2 \cdot 10^{-2}$ ,  $2 \cdot 10^{-3}$ ,  $2 \cdot 10^{-4}$  and  $5 \cdot 10^{-7} G_0$  for Ti, Au,  $G_{\text{cov}}$  and  $G_{\text{vdW}}$ , respectively. From these

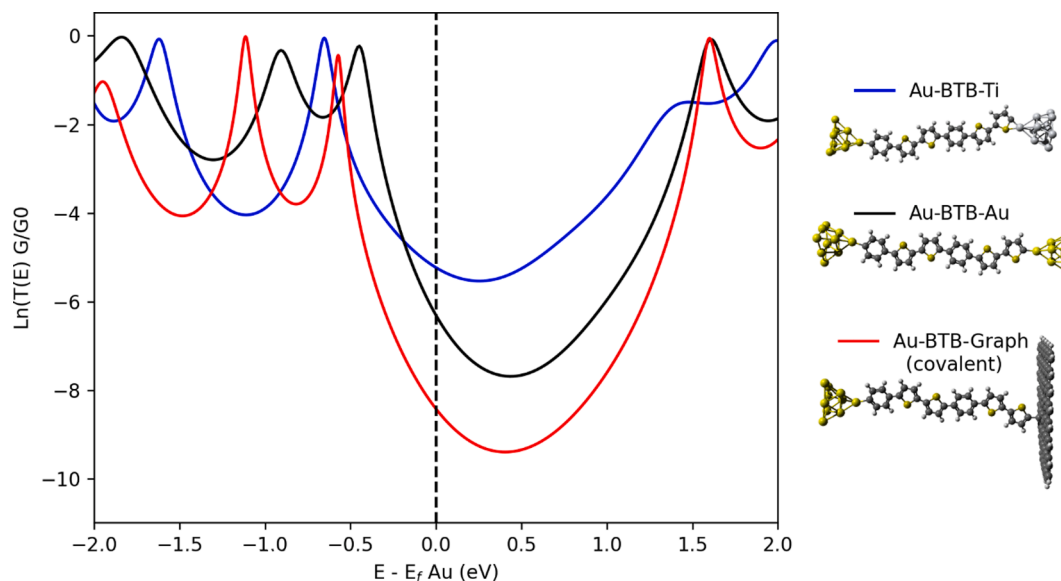


**Fig. 2.** Variation of  $T(E)$  of  $(BTB)_2$  for different right electrodes.

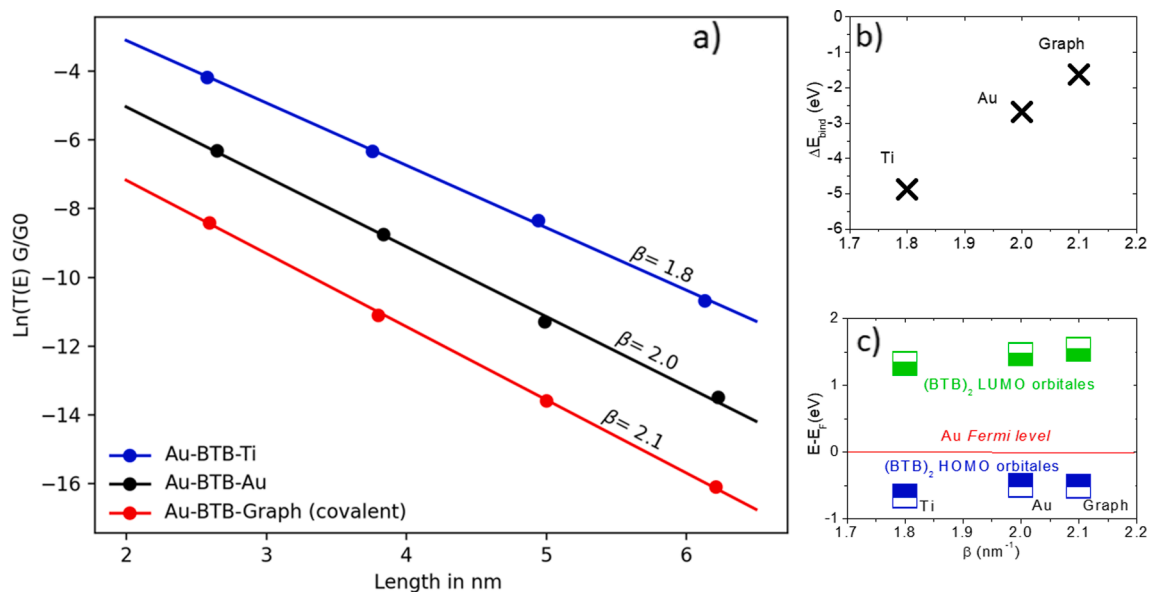


**Fig. 3.** Log ( $T(E_F)$ ) at zero bias as a function of the molecular junction length (a); variation of  $\Delta E_{bind}$  relative to attenuation factor  $\beta$  (b); HOMO and LUMO orbitals in function of  $\beta$  (c).

results, we can deduce that the coupling to the titanium electrode leads to the highest probability of electronic transmission. It is followed by gold and graphene covalently bonded to BTB. The lowest transmittance is observed for the case where the BTB is weakly bonded to graphene through van der Waals interactions. In this last case, an additional tunnel barrier is added between the electrodes due to the lack of a support channel between the anchoring unit and the graphene electrode.

In Fig. 3a, the transmittance value at Fermi level ( $T(E_F)$ ) is plotted as a function of the molecular length, varying from 1 to 5 BTB units. As a result, all these asymmetric junctions provide a linear decrease (on a logarithmic scale) of conductance in the non-resonant tunneling transport mechanism.

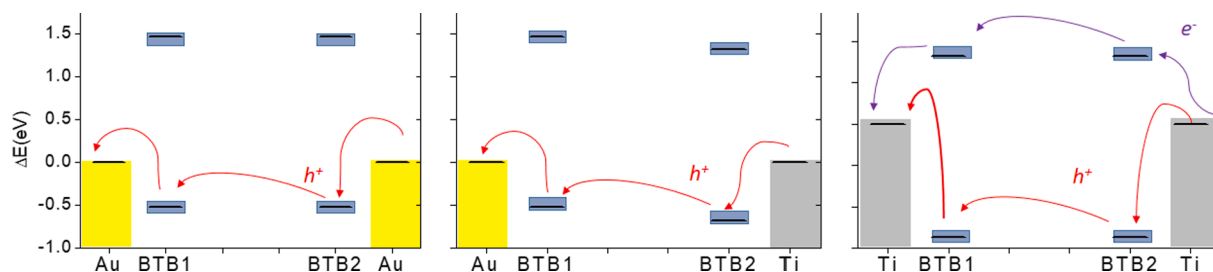
The slopes of the curves represent the attenuation factor  $\beta$ : 1.8, 2.0 and  $2.1 \text{ nm}^{-1}$  for Ti, Au and  $G_{\text{graph}}$  respectively. The calculated value for Ti is in a good agreement with experimental measurements[41] ( $1.8 \text{ nm}^{-1}$ ). McCreery *et al.*[20] found a  $\beta$  value around  $2.9 \text{ nm}^{-1}$  for  $G\text{-(BTB)}_n\text{-G}$ , which is similar to  $\text{Au-(BTB)}_n\text{-G}_{\text{graph}}$  ( $2.1 \text{ nm}^{-1}$ ) and  $\text{Au-(BTB)}_n\text{-Au}$  ( $2.0 \text{ nm}^{-1}$ ) presented on Fig. 3. The decay constant depends on both the coupling between electrodes and anchoring groups (type and strength) and the frontier orbital (HOMO, LUMO) positions.

In Fig. 3b, the variation of the binding energy ( $\Delta E_{bind}$ ) with the decay constant shows that the higher  $\Delta E_{bind}$ , the lower is  $\beta$ , in agreement with the conclusions of the recent review on molecular junctions, which claims that  $\beta$  depends mainly on the strongly coupled electrode.[18] Indeed, for stronger coupling, one can expect a better conduction, in agreement with the transmittance value at the Fermi level presented above. The lowest constant is found for the Ti electrode with a binding energy of  $-4.885 \text{ eV}$  and the highest for graphene with a binding energy

of  $-1.623 \text{ eV}$  in the same order of magnitude of previous molecules chemisorbed on graphitic systems[42,43] and lower than the non-covalently adsorbed molecules on graphene[44,45]. While there is no result in the literature on molecular adsorption on Ti surfaces, the binding energy obtained for benzene on  $G_{\text{cov}}$  is  $-1.617 \text{ eV}$ , in agreement with the literature.[42] On Au (111) surface, it is  $-2.674 \text{ eV}$ , in agreement with previous studies[46,47].

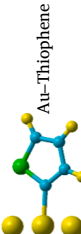
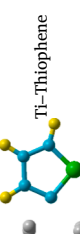
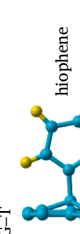
Fig. 3c presents the position of the lowest unoccupied orbital (LUMO) of  $(\text{BTB})_2$  which is located at 1.46, 1.32 and 1.53 eV above Fermi energy level ( $E_F$ ) for Au, Ti and  $G_{\text{cov}}$ , respectively. The highest occupied orbital (HOMO) is located at 0.51, 0.67 and 0.52 eV below  $E_f$  for Au, Ti and  $G_{\text{graph}}$ , respectively. The LUMO of Ti is close to the Fermi level, making it the best conduction channel in the case of  $\text{Au-(BTB)}_2\text{-Ti}$ . This means that the coupling to the electrode has an influence on the acceptor/donor character in the molecular junction.

From these results, one can observe that the relation  $\Delta E_{bind}$  versus  $\beta$  appears to be linear respecting the interaction strength with the molecule and the coupling of Fermi level with the frontier orbitals of BTB (Fig. 4). The total density of states (DOS) projected onto the d-valence orbitals of Ti ( $d_{Ti}$ ) and Au ( $d_{Au}$ ) (Figure S3) shows for  $d_{Ti}$  a broad band that covers both HOMO and LUMO around the Fermi level while  $d_{Au}$  interact merely with the HOMO below the Fermi level. We changed the positions of the Au and Ti electrodes and studied a symmetrical junction with only Ti electrodes. The corresponding results (Figures S1 and S2) support the hypothesis of a stronger interaction of titanium with BTB resulting in a displacement of LUMO toward the Fermi level of titanium. These observations are in agreement with the difference in electronegativity between Ti and carbon, suggesting an electron transfer from



**Fig. 4.** Position of  $(\text{BTB})_2$  HOMO and LUMO orbitals relative to metal Fermi levels for  $\text{Au-(BTB)}_2\text{-Au}$  (a),  $\text{Au-(BTB)}_2\text{-Ti}$  (b) and  $\text{Ti-(BTB)}_2\text{-Ti}$  (c).

**Table 2**  
Adsorption energies, thiophene-surface distance, bare metal ( $\Phi_{\text{surface}}$ ) and complex ( $\Phi_{\text{sam}}$ ) work functions,  $\Delta V_m$  and BDE for Au, Ti and G electrodes.

Metal-Molecule	Binding energy (eV)	C-M bond length (Å)	Sum of covalent radii (Å)	Ionic character(%)	$\Phi_{\text{surface}}$ (eV)	$\Phi_{\text{sam}}$ (eV)	$\Delta\Phi$ (eV)	$\Delta V_m$	BD
 Au-Thiophene	-3.183	2.041	1.99	2.5	5.19	5.11	-0.08	-0.01	-0.07
 Ti-Thiophene	-4.885	2.37	2.11	11.1	4.37	4.09	-0.28	-0.01	-0.27
 G-T	-1.623	1.56	1.50	3.2	4.22	4.25	0.03	-0.01	0.04

titanium to the carbon atom of BTB. This charge transfer process is investigated in the next section.

### 3.3. Analysis of the nature OF Au/Ti/G-C BONDING

The similar behavior observed in the case of Au and Graph can be explained by the nature of the chemical interaction between the electrode and the anchoring group. Indeed, by calculating the Bader atomic charges and the differences in charge densities (Table S2), we have shown that the Ti-thiophene bond is covalent with a significant ionic character. Indeed, calculations show a charge transfer from Ti to the molecule (0.5 e-) in agreement with the shift of LUMO position toward Fermi level energy.

Conversely, for gold or graphene charge transfer with the anchoring group is weak. These results are in line with the difference in electronegativities. The electronegativity difference between titanium and carbon is 1.05 while it is 0.01 between gold and carbon.

These results prove that the Ti-C bond presents significant ionic-covalent character, while the ionic character of the Au-C bond is weak. We have calculated the variation of the metal work function due to its interaction with the anchoring group. It was shown and largely discussed in the literature[48] that this variation can be decomposed into two terms[49]:  $\Delta\Phi = \Delta V_m + \text{BDE}$ , where  $\Delta V_m$  is the variation of the potential between the anchoring group and the top of the molecule, and BDE (Binding dipole Energy) is the potential variation due to charge redistribution between the anchoring group and the metal surface. The two quantities were computed at the DFT level and the results are reported in Table 2. As can be seen, the BDE value is close to zero for Au and graphene electrodes, in agreement with the lack of a local dipole at the interface, because of the similar electronegativities of the binding atoms. However, the BDE value is -0.35 eV for the Ti electrode, consistent with the observed charge transfer between Ti and C atoms. This corresponds to a strong surface dipole due the charge redistribution at metal molecule interface.

This redistribution coupled to the shift of LUMO may be at the origin of the asymmetry of the electronic current observed previously for Au-(BTB)<sub>n</sub>-Ti junction[48,50] was demonstrated experimentally. Our calculations provide qualitative and quantitative informations supporting the assumptions made about the coupling strength and the positions of the frontier orbitals relative to the Fermi level. Indeed, strong adsorption energies are found for anchoring groups on Au and Ti surfaces. The Fig. 4a presents the position of HOMO and LUMO of BTB relative to Au Fermi level showing a gap of 0.52 and 1.46 eV, respectively. This indicates that the preferential conduction channel would be the HOMO highlighting a mechanism of conduction by hole. The Fig. 4b exhibits same information for the asymmetric Au-(BTB)<sub>2</sub>-Ti junction. In this case, the LUMO moves toward Fermi level ( $E_F$ ) of titanium, while the HOMO shifts away from. The gap becomes 1.32 eV between LUMO and  $E_F$ , and 0.67 eV between HOMO and  $E_F$ . The preferential conduction channel remains the HOMO predicting a mechanism of conduction by hole. In the case of Ti-(BTB)<sub>2</sub>-Ti junction, as it can be seen on Fig. 4c the gaps HOMO- $E_F$  and LUMO- $E_F$  are 1.37 and 0.82 eV, respectively. The shift of the LUMO toward  $E_F$  is in agreement with the observed charge transfer from Ti to BTB molecule anchoring group. In this latter case, a conduction mechanism through electrons becomes probable even if it may be minority.

## 4. Conclusion

In this work, we have implemented a fast and accurate methodology, to determine the transport properties of large molecular junctions, within the DFT formalism coupled to NEGF using the Fisher-Lee formalism. A comparison with both experiment and other theoretical methodologies shows that this approach is very efficient.

We use this methodology to explore the geometries and electron transport properties of BTB oligomers sandwiched between gold,

titanium and graphene electrodes. The calculated values of the attenuation factor  $\beta$  are in a good agreement with experimental results. To the best of our knowledge, this is the first theoretical study on asymmetric X-(BTB)<sub>n</sub>-Y (X, Y = Au, Ti, G<sub>cov</sub> and G<sub>vdW</sub>) molecular junctions. The calculated attenuation factor for the Au-(BTB)<sub>n</sub>-Ti and G-(BTB)<sub>n</sub>-G junction are found to 1.8 and 2.1 nm<sup>-1</sup>, respectively, very close to the experimental ones. The variation of  $\beta$  depends slightly on the asymmetry of the electrodes and strongly on the nature and strength of the metal-molecule interaction. It roughly follows the calculated binding energies of molecules on metals. Analysis of the nature of the molecular bond shows that gold and graphene form the same type of quasi-covalent bond, in agreement with their respective electronegativities. For titanium, we have found a charge transfer mechanism from the metal to the molecule in agreement with a very high interface dipole and the shift of the LUMO toward Fermi level. These results provide insights and rationalize the transport mechanism studied experimentally for the Au-(BTB)<sub>n</sub>-Ti junction and predicts a possible combined electron and hole transport mechanism for Ti-(BTB)<sub>n</sub>-Ti.

## 5. Supporting Information

Variation of  $T(E)$  of (BTB)<sub>2</sub> for X-(BT B)<sub>2</sub>-Y (X, Y = Au, Ti, G<sub>cov</sub> and G<sub>vdW</sub>); Variation of  $T(E_F)$  as a function of molecular length for different electrodes; Partial density of states of Au Ti and BTB; Comparison of experimental and calculated contact resistances; Bader charges analysis on binding sites and the difference in charge densities indicating the regions of charge accumulation and depletion.

## Declaration of Competing Interest

The authors declare that they have no known competing financial interests or personal relationships that could have appeared to influence the work reported in this paper.

## Acknowledgements

Quantum chemical calculations were performed using HPC resources from GENCI- [CCRT/CINES/IDRIS] (Grant 2020[A0080807006]. ANR (Agence Nationale de la Recherche) and CGI (Commissariat à l'Investissement d'Avenir) are gratefully acknowledged for their financial support of this work through LabEX SEAM (Science and Engineering for Advanced Materials and devices): ANR-10-LABX-096 and ANR-18-IDEX-0001.

## Appendix A. Supplementary material

Supplementary data to this article can be found online at <https://doi.org/10.1016/j.cplett.2021.139273>.

## References

- M. Lieberman, A Crash Course in Molecular Electronics, in: Mol. Compon. Electron. Devices, American Chemical Society, 2003: pp. 1–8. [10.1021/bk-2003-0844.ch001](https://doi.org/10.1021/bk-2003-0844.ch001).
- T. Rakshit, G.-C. Liang, A.W. Ghosh, S. Datta, Silicon-based Molecular Electronics, Nano Lett. 4 (10) (2004) 1803–1807, <https://doi.org/10.1021/nl049436t>.
- T. Stuyver, T. Zeng, Y. Tsuji, S. Fias, P. Geerlings, F. De Proft, Captodative Substitution: A Strategy for Enhancing the Conductivity of Molecular Electronic Devices, J. Phys. Chem. C. 122 (2018) 3194–3200, <https://doi.org/10.1021/acs.jpcc.7b10877>.
- I. Rungger, S. Sanvito, Algorithm for the construction of self-energies for electronic transport calculations based on singularity elimination and singular value decomposition, Phys Rev B. 78 (2008), 035407, <https://doi.org/10.1103/PhysRevB.78.035407>.
- J.J. Palacios, E. Louis, A.J. Pérez-Jiménez, E. San Fabián, J.A. Vergés, An ab initio approach to electrical transport in molecular devices, Nanotechnology. 13 (2002) 378.
- G.C. Solomon, D.Q. Andrews, R.P. Van Duyne, M.A. Ratner, Electron Transport through Conjugated Molecules: When the  $\pi$  System Only Tells Part of the Story, ChemPhysChem. 10 (2009) 257–264, <https://doi.org/10.1002/cphc.200800591>.
- P. Roy, S. Biswas, A. Pramanik, P. Sarkar, Substitution induced carrier switching in S, N-heteroacene molecular junctions: A first principle analysis, Chem. Phys. Lett. 708 (2018) 87–93, <https://doi.org/10.1016/j.cplett.2018.08.007>.
- Z. Xie, X.-L. Ji, Y. Song, M.-Z. Wei, C.-K. Wang, More aromatic molecular junction has lower conductance, Chem. Phys. Lett. 639 (2015) 131–134, <https://doi.org/10.1016/j.cplett.2015.09.017>.
- D.J. Sandman, A Review of: "Handbook of Thiophene-Based Materials: Applications in Organic Electronics and Photonics, Vols. 1 and 2, I. F. Perepichka & D. F. Perepichka," Mol. Cryst. Liq. Cryst. 528 (2010) 193–194. [10.1080/15421406.2010.505257](https://doi.org/10.1080/15421406.2010.505257).
- R. Yamada, H. Kumazawa, T. Noutoshi, S. Tanaka, H. Tada, Electrical conductance of oligothiophene molecular wires, Nano Lett. 8 (4) (2008) 1237–1240.
- T. Ohto, T. Inoue, H. Stewart, Y. Numai, Y. Aso, Y. Ie, R. Yamada, H. Tada, Effects of cis-trans Conformation between Thiophene Rings on Conductance of Oligothiophenes, J. Phys. Chem. Lett. 10 (18) (2019) 5292–5296, <https://doi.org/10.1021/acs.jpcllett.9b02059>.
- B. Capozzi, E.J. Dell, T.C. Berkelbach, D.R. Reichman, L. Venkataraman, L. M. Campos, Length-dependent conductance of oligothiophenes, J. Am. Chem. Soc. 136 (29) (2014) 10486–10492.
- E. Leary, H. Höbenreich, S.J. Higgins, H. van Zalinge, W. Haiss, R.J. Nichols, C. M. Finch, I. Grace, C.J. Lambert, R. McGrath, J. Smerdon, Single-Molecule Solvation-Shell Sensing, Phys Rev Lett. 102 (2009), 086801, <https://doi.org/10.1103/PhysRevLett.102.086801>.
- L. Xiang, T. Hines, J.L. Palma, X. Lu, V. Mujica, M.A. Ratner, G. Zhou, N. Tao, Non-exponential length dependence of conductance in iodide-terminated oligothiophene single-molecule tunneling junctions, J. Am. Chem. Soc. 138 (2) (2016) 679–687.
- X. Li, Q. Wu, J. Bai, S. Hou, W. Jiang, C. Tang, H. Song, X. Huang, J. Zheng, Y. Yang, J. Liu, Y. Hu, J. Shi, Z. Liu, C.J. Lambert, D. Zhang, W. Hong, Structure-Independent Conductance of Thiophene-Based Single-Stacking Junctions, Angew. Chem. Int. Ed Engl. 59 (8) (2020) 3280–3286, <https://doi.org/10.1002/anie.v59.8>.
- D.S. Fisher, P.A. Lee, Relation between conductivity and transmission matrix, Phys. Rev. B. 23 (1981) 6851.
- J.P. Lewis, P. Jelínek, J. Ortega, A.A. Demkov, D.G. Trabada, B. Haycock, H. Wang, G. Adams, J.K. Tomfohr, E. Abad, Advances and applications in the FIREBALL ab initio tight-binding molecular-dynamics formalism, Phys. Status Solidi B. 248 (2011) 1989–2007.
- Y.J. Dappe, Attenuation Factors in Molecular Electronics: Some Theoretical Concepts, Appl. Sci. 10 (2020) 6162.
- C. Zhai, D. Hanaor, G. Proust, L. Brassart, Y. Gan, Interfacial electro-mechanical behaviour at rough surfaces, Mech. Energy Mater. 9 (2016) 422–429, <https://doi.org/10.1016/j.eml.2016.03.021>.
- H. Yan, A.J. Bergren, R. McCreery, M.L. Della Rocca, P. Martin, P. Lafarge, J. C. Lacroix, Activationless charge transport across 4.5 to 22 nm in molecular electronic junctions, Proc. Natl. Acad. Sci. 110 (14) (2013) 5326–5330, <https://doi.org/10.1073/pnas.1221643110>.
- M.A. Basanta, Y.J. Dappe, P. Jelínek, J. Ortega, Optimized atomic-like orbitals for first-principles tight-binding molecular dynamics, Comput. Mater. Sci. 39 (4) (2007) 759–766.
- P. Jelínek, H. Wang, J.P. Lewis, O.F. Sankey, J. Ortega, Multicenter approach to the exchange-correlation interactions in ab initio tight-binding methods, Phys. Rev. B. 71 (2005), 235101.
- M. Seydou, Y.J. Dappe, S. Marsaudon, J.-P. Aimé, X. Bouju, A.-M. Bonnot, Atomic force microscope measurements and  $\rho$  calculations of contact length between a carbon nanotube and a graphene surface, Phys Rev B. 83 (2011), 045410, <https://doi.org/10.1103/PhysRevB.83.045410>.
- D. Pierucci, H. Henck, Z. Ben Aziza, C.H. Naylor, A. Balan, J.E. Rault, M.G. Silly, Y. J. Dappe, F. Bertran, P. Le Fèvre, F. Sirotti, A.T.C. Johnson, A. Ouerghi, Tunable Doping in Hydrogenated Single Layered Molybdenum Disulfide, ACS Nano. 11 (2) (2017) 1755–1761, <https://doi.org/10.1021/acsnano.6b07661>.
- C. González, E. Abad, Y.J. Dappe, J.C. Cuevas, Theoretical study of carbon-based tips for scanning tunnelling microscopy, Nanotechnology. 27 (2016), 105201.
- Q. Zhang, L. Liu, S. Tao, C. Wang, C. Zhao, C. González, Y.J. Dappe, R.J. Nichols, L. i. Yang, Graphene as a Promising Electrode for Low-Current Attenuation in Nonsymmetric Molecular Junctions, Nano Lett. 16 (10) (2016) 6534–6540, <https://doi.org/10.1021/acs.nanolett.6b03180>.
- J.P. Perdew, K. Burke, M. Ernzerhof, Phys Rev Lett. 78 (1997) 1396.
- G. Kresse, J. Hafner, Ab initio molecular dynamics for liquid metals, Phys Rev B. 47 (1) (1993) 558–561, <https://doi.org/10.1103/PhysRevB.47.558>.
- G. Kresse, D. Joubert, From ultrasoft pseudopotentials to the projector augmented-wave method, Phys Rev B. 59 (3) (1999) 1758–1775, <https://doi.org/10.1103/PhysRevB.59.1758>.
- S. Grimme, J. Antony, S. Ehrlich, H. Krieg, A consistent and accurate ab initio parametrization of density functional dispersion correction (DFT-D) for the 94 elements H-Pu, J. Chem. Phys. 132 (2010), 154104, <https://doi.org/10.1063/1.3382344>.
- B. Diawara, <http://modelview.fr/fr.html>, ENSCP, PSL Paris, n.d.
- Parameter Tables of Crystals, in: Crystallogr. Surf. Struct., John Wiley & Sons, Ltd, 2016: pp. 351–353. [10.1002/9783527697137.app2](https://doi.org/10.1002/9783527697137.app2).
- J. Zemann, Crystal structures, 2nd edition. Vol. 1 by R. W. G. Wyckoff, Acta Crystallogr. 18 (1965) 139–139. [10.1107/S0365110X65000361](https://doi.org/10.1107/S0365110X65000361).
- M. Yu, D.R. Trinkle, Accurate and efficient algorithm for Bader charge integration, J. Chem. Phys. 134 (2011), 064111, <https://doi.org/10.1063/1.3553716>.



- [35] C.E. Smith, S.O. Odoh, S. Ghosh, L. Gagliardi, C.J. Cramer, C.D. Frisbie, Length-Dependent Nanotransport and Charge Hopping Bottlenecks in Long Thiophene-Containing  $\pi$ -Conjugated Molecular Wires, *J. Am. Chem. Soc.* 137 (50) (2015) 15732–15741, <https://doi.org/10.1021/jacs.5b07400>, <https://doi.org/10.1021/jacs.5b07400.s001>.
- [36] D.J. Wold, R. Haag, M.A. Rampi, C.D. Frisbie, Distance dependence of electron tunneling through self-assembled monolayers measured by conducting probe atomic force microscopy: Unsaturated versus saturated molecular junctions, *J. Phys. Chem. B.* 106 (2002) 2813–2816.
- [37] P. Moreno-García, M. Gulcur, D.Z. Manrique, T. Pope, W. Hong, V. Kaliginedi, C. Huang, A.S. Batsanov, M.R. Bryce, C. Lambert, Single-molecule conductance of functionalized oligoynes: Length dependence and junction evolution, *J. Am. Chem. Soc.* 135 (2013) 12228–12240.
- [38] S. Ho Choi, BongSoo Kim, C.D. Frisbie, Electrical resistance of long conjugated molecular wires, *Science*. 320 (5882) (2008) 1482–1486.
- [39] H. Liu, Z. Zhao, N. Wang, C. Yu, J. Zhao, Can the transition from tunneling to hopping in molecular junctions be predicted by theoretical calculation? *J. Comput. Chem.* 32 (8) (2011) 1687–1693.
- [40] Y. He, N. Cheng, J. Zhao, First-principle study on the conductance of benzene-based molecules with various bonding characteristics, *Comput. Theor. Chem.* 1154 (2019) 1–10, <https://doi.org/10.1016/j.comptc.2019.03.006>.
- [41] Q.V. Nguyen, P. Martin, D. Frath, M.L. Della Rocca, F. Lafolet, S. Bellinck, P. Lafarge, J.-C. Lacroix, Highly Efficient Long-Range Electron Transport in a Viologen-Based Molecular Junction, *J. Am. Chem. Soc.* 140 (32) (2018) 10131–10134.
- [42] S. Rahali, Y. Belhocine, J. Touzeau, B. Tangour, F. Maurel, M. Seydou, Balance between physical and chemical interactions of second-row diatomic molecules with graphene sheet, *Superlattices Microstruct.* 102 (2017) 45–55, <https://doi.org/10.1016/j.spmi.2016.12.015>.
- [43] M. Lo, M. Seydou, A. Bensghaier, R. Pires, D. Gningue-Sall, J.-J. Aaron, Z. Mekhalif, J. Delhalle, M.M. Chehimi, Polypyrrole-Wrapped Carbon Nanotube Composite Films Coated on Diazonium-Modified Flexible ITO Sheets for the Electroanalysis of Heavy Metal Ions, *Sensors*. 20 (2020), <https://doi.org/10.3390/s20030580>.
- [44] A. Quesne-Turin, J. Touzeau, Y.J. Dappe, B. Diawara, F. Maurel, M. Seydou, First-principles investigation of the structural and electronic properties of self-assemblies of functional molecules on graphene, *Superlattices Microstruct.* 105 (2017) 139–151, <https://doi.org/10.1016/j.spmi.2017.03.034>.
- [45] J. Touzeau, F. Barbault, F. Maurel, M. Seydou, Insights on porphyrin-functionalized graphene: Theoretical study of substituent and metal-center effects on adsorption, *Chem. Phys. Lett.* 713 (2018) 172–179, <https://doi.org/10.1016/j.cplett.2018.10.046>.
- [46] A. Berisha, C. Combella, F. Kanoufi, J. Médard, P. Decorse, C. Mangeney, I. Kherbouche, M. Seydou, F. Maurel, J. Pinson, Alkyl-Modified Gold Surfaces: Characterization of the Au–C Bond, *Langmuir*. 34 (2018) 11264–11271, <https://doi.org/10.1021/acs.langmuir.8b01584>.
- [47] D. Nassoko, M. Seydou, C. Goldmann, C. Chanéac, C. Sanchez, D. Portehault, F. Tielens, Rationalizing the formation of binary mixed thiol self-assembled monolayers, *Mater. Today Chem.* 5 (2017) 34–42, <https://doi.org/10.1016/j.mtchem.2017.05.002>.
- [48] G. Heimel, L. Romaner, E. Zojer, J.-L. Brédas, Toward Control of the Metal–Organic Interfacial Electronic Structure in Molecular Electronics: A First-Principles Study on Self-Assembled Monolayers of  $\pi$ -Conjugated Molecules on Noble Metals, *Nano Lett.* 7 (2007) 932–940, <https://doi.org/10.1021/nl0629106>.
- [49] I.H. Campbell, S. Rubin, T.A. Zawodzinski, J.D. Kress, R.L. Martin, D.L. Smith, N. N. Barashkov, J.P. Ferraris, Controlling Schottky energy barriers in organic electronic devices using self-assembled monolayers, *Phys Rev B.* 54 (1996) R14321–R14324, <https://doi.org/10.1103/PhysRevB.54.R14321>.
- [50] Z. Xie, I. Baldea, C.E. Smith, Y. Wu, C.D. Frisbie, Experimental and Theoretical Analysis of Nanotransport in Oligophenylene Dithiol Junctions as a Function of Molecular Length and Contact Work Function, *ACS Nano*. 9 (8) (2015) 8022–8036, <https://doi.org/10.1021/acsnano.5b01629>.